communications physics

Article

https://doi.org/10.1038/s42005-024-01908-y

Quantum origin of anomalous Floquet phases in cavity-QED materials

Check for updates

Beatriz Pérez-González [1,2] ✉, Gloria Platero[1] ✉ & Álvaro Gómez-León[3] ✉

Anomalous Floquet topological phases are unique to periodically driven systems, lacking a static analog. Inspired by Floquet Engineering with classical electromagnetic radiation, Quantum Floquet Engineering has emerged as a promising tool to tailor the properties of quantum materials using quantum light. While the latter recovers the physics of Floquet materials in its semi-classical limit, the mapping between these two scenarios remains mysterious in many aspects. In this work, we discuss the emergence of quantum anomalous topological phases in cavity-QED materials, linking the topological phase transitions in the electron-photon spectrum with those in the 0- and π-gaps of Floquet quasienergies. Our results establish the microscopic origin of an emergent discrete time-translation symmetry in the matter sector, and link isolated c-QED materials with periodically driven ones. Finally, we discuss the bulk-edge correspondence in terms of hybrid light-matter topological invariants.

Topological systems in condensed matter have attracted wide attention during the last decades. Their robust and exotic physical properties, which can be characterized using simple topological arguments[1,2], have found a wide number of applications[3–5].

In particular, topological systems in periodically driven (Floquet) set-ups have gained special attention[6–12]. Initially, they were in the spotlight for their external control, which allowed them to simulate complex static topological phases. However, the discovery of anomalous Floquet topological phases[13–17], a unique phenomenon of periodically driven systems where a system with topologically trivial bands displays topologically protected edge states, renewed the interest in their topology.

Simultaneously, the research in cavity-QED (c-QED) materials is booming due to recent experimental advances that allow to explore new regimes of light-matter interaction[18–21]. In this case, the material couples to quantized light and forms an isolated hybrid state with properties dictated by the mutual influence between electrons and photons. Here, the interest is not only to understand the fundamental interactions between light and matter but also to tame these interactions for their use in quantum technologies[22,23].

The link between c-QED materials and Floquet physics is currently being unfolded. It has been demonstrated that the semi-classical limit of c-QED materials features aspects of Floquet physics, such as the band renormalization by Bessel functions[24]. Attempts to further understand this emergence of an effective Floquet description in the semi-classical limit of c-QED materials have given birth to Quantum Floquet engineering[25–30]. Intuitively, their relation can be understood from the point of view that, if a cavity field in its steady state is traced out, the matter effectively couples to a time-periodic drive with frequency set by the cavity. However, for this to be true, both the back-action from the matter onto the cavity field and the light-matter correlations must be negligible. This defines the semi-classical limit of c-QED materials where one effectively obtains the physics of Floquet systems[24,31].

This relation is not a mere curiosity and has profound implications. It stems from the fact that there is a microscopic mechanism by which the discrete time-translation symmetry of Floquet systems $H(t) = H(t+T)$, effectively emerges from the isolated photon-electron quantum system[32]. It also provides a bridge between widely different conserved quantities: the energies of the c-QED material and the quasienergies of the Floquet system, which are notably defined modulo 2π only.

In this work, we shed light into these questions by asking: *what is the microscopic origin of anomalous Floquet topological phases?* Can we extend the mapping between quantum and classical light to seek anomalous Floquet phases in electron-photon systems? Notice that the existence of anomalous Floquet phases strongly depends on the hypothesis of time periodicity, and it is because of this symmetry that their topological classification goes beyond that of static systems[33].

We show that anomalous topological phases can emerge in c-QED materials when the cavity mode is resonant with the band transitions of a topological system. If this resonant interaction has the right symmetries, it opens additional gaps between distinct photonic bands that contain edge states, and in contrast with the original ones, they are made of entangled light-matter excitations. We find that despite the existence of these

[1]Instituto de Ciencia de Materiales de Madrid (ICMM), CSIC, Madrid, Spain. [2]Institute of Physics, University of Augsburg, Augsburg, Germany. [3]Institute of Fundamental Physics IFF-CSIC, Madrid, Spain. ✉e-mail: perezg.bea@gmail.com; gplatero@icmm.csic.es; a.gomez.leon@csic.es

additional edge states, the topological invariant for the interacting system vanishes, invalidating the bulk-boundary correspondence, in analogy with the anomalous topology of Floquet phases. To resolve this, we demonstrate that it is possible to assign two topological invariants to the system and through them, establish a bulk-boundary correspondence that perfectly predicts the existence of edge states. Furthermore, the existence of these pair of invariants allows us to identify the π-gap of Floquet systems with the gaps opened by this resonant interaction, establishing a link between cavity-QED materials and periodically driven systems.

Results and discussion

Model Hamiltonian

The Su-Schrieffer-Heeger (SSH) model has been a canonical model of a topological insulator in one dimension for a long time[34–37]. Not only its topology in the static case has been studied, but also its periodically driven version has been used to analyze Floquet phases[8, 38–40]. For example, when coupled to light via the Peierls substitution, one can easily show the control of topological edge states at high-frequency[12]. The Peierls substitution implies the photo-dressing of the hopping amplitudes J_{ij} connecting sites i and j through $J_{ij} \to J_{ij}\exp\{-i\int_{i\to j}A(r,t)dr\}$, where $A(r,t)$ is the vector potential associated with the time-periodic field. Usually, the amplitude of the vector potential is taken to be constant, $A_0 \neq A_0(t)$. As a further revision is out of the scope of the present work, we suggest the reader check reference[41].

However, genuinely new phases of the Floquet-driven system emerge for low driving frequency and particular driving protocols that are resonant with the system[42]. To fully understand this, let us very briefly review the basics of Floquet theory for (semi-classically) driven topological systems. For a given time-periodic Hamiltonian, $H(t) = H(t+T)$ (with T being the driving period), Floquet theory tells us that the corresponding time-dependent Schrödinger equation $i\partial_t|\chi(t)\rangle = H(t)|\chi(t)\rangle$ has generalized Floquet solutions $|\chi(t)\rangle$ of the form $|\chi(t)\rangle = e^{-i\varepsilon t}|u(t)\rangle$. Here, $|u(t)\rangle$ are the so-called Floquet states, which inherit the time periodicity of the driving field, $|u(t)\rangle = |u(t+T)\rangle$, while the phase ε is the quasienergy, the conserved quantity in driven systems that takes the role of the energy in static ones. Importantly, the quasienergy spectrum can be defined up to an integer multiple of the driving frequency $\omega = 2\pi/T$, $\varepsilon \to \varepsilon + n\omega$, which does not change the corresponding Floquet state $|u(t)\rangle$. Hence, the quasienergy spectrum of the driven system is made out of infinitely many replicas, known as Floquet replicas, separated by ω. Each replica contains a finite set of independent quasienergies and Floquet states $\{\varepsilon_j, |u(t)\rangle\}$, with index j running up to the dimension of the driven quantum material.

The quasienergy spectrum contains two inequivalent gaps: the 0-gap, which appears within a given Floquet replica, and the π − gap appearing between adjacent replicas due to the repeating structure. Hence, this second gap is specific for time-periodic driven systems, and when the driving frequency is reduced, it can be closed and reopened through a topological phase transition. In such cases, both gaps could host topological edge states, while the winding number of the quasienergy bands remains trivial[17, 43, 44]. Such topological phases are called anomalous[13, 45], and cannot be properly captured by an effective static matter Hamiltonian or, equivalently, a stroboscopic description of the system dynamics.

This coexistence of topological edge states with topologically trivial Floquet bands is a hallmark of Floquet phases lacking a static analog. For this reason, if Floquet phases are to arise from c-QED materials in a semi-classical limit, it is important to understand their quantum origin. For that, we study an SSH chain interacting with a single-mode cavity via the following photon-assisted hopping (see Fig. 1):

$$H = \Omega d^\dagger d + \sum_{j=1}^{N}\left(J_1[d]b_j^\dagger a_j + J_2[d]a_{j+1}^\dagger b_j + \text{h.c.}\right), \tag{1}$$

where we have defined the photon-assisted hopping $J_1[d] \equiv J + g\left(d + d^\dagger\right)$ and $J_2[d] \equiv J' - g\left(d + d^\dagger\right)$. The first term in Eq. (1) describes a cavity with

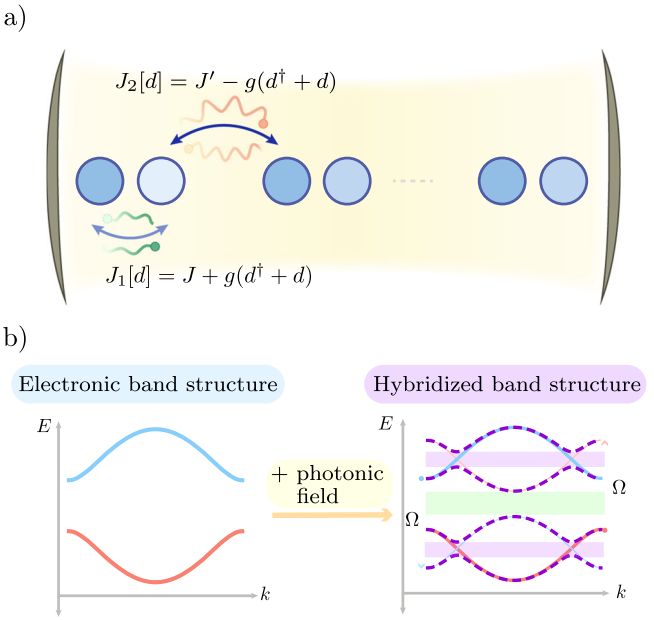

Fig. 1 | Schematic figure of the total system. a The SSH chain interacts with the cavity field through the photon-assisted hopping, as described by Eq. (1). **b** When the coupling to a resonant cavity is added, the hybridized band structure showcases anomalous gaps (violet) and single-particle gaps (green), which can be both populated by topological edge states (right), as opposed to the band structure of the isolated chain (left), in which only single-particle edge states can appear.

frequency Ω and photon operators d and $d^\dagger$, while the second term describes the hopping of spinless fermions between sites A and B of the chain with operators a_j, $a_j^\dagger$, b_j and $b_j^\dagger$. Importantly, the hopping in the chain is not only dimerized with J and J', but also modulated by the absorption/emission of photons, with opposite signs for the intra- and inter-dimer hopping. Some experimental works have demonstrated the coexistence of these inequivalent topological edge states in the gaps of driven SSH chains, in the semi-classical regime[44, 46]. In this case, the driving protocol also has the form of a hopping modulation, with $J_1(t) = J_1 + 2V\cos(\omega t)$ and $J_2(t) = J_2 - 2V\cos(\omega t)$, where V is the driving amplitude. Note that the sign change between $J_1(t)$ and $J_2(t)$ is mimicked by $J_1[d]$ and $J_2[d]$ in the quantum version of Eq. (1).

As Eq. (1) describes a complex problem, let us first introduce the basic properties of the unperturbed SSH chain Hamiltonian $H_{\text{SSH}} = H(g=0)$. For Periodic Boundary Conditions (PBC), the chain Hamiltonian can be exactly diagonalized and results in two eigenstates, $|\varphi_\pm(k)\rangle$, with energies:

$$E_\pm(k) = \pm\sqrt{J^2 + J'^2 + 2JJ'\cos(k)}. \tag{2}$$

The topology can be characterized by the Zak phase, which is obtained by integrating the Berry connection $A^0_{\mu,\mu}$ over the FBZ[47–49]:

$$\gamma_0 = \int_{-\pi}^{\pi}\mathcal{A}^0_{\mu,\mu}(k)dk = \int_{-\pi}^{\pi}\langle\varphi_\mu(k)|i\partial_k|\varphi_\mu(k)\rangle\, dk, \tag{3}$$

where $|\phi_\mu(k)\rangle$ ($\mu = \pm$) are the eigenstates of the unperturbed SSH chain. Due to chiral symmetry, $\sigma_z H_{\text{SSH}}(k)\sigma_z = -H_{\text{SSH}}(k)$ (where σ_z is written in the basis of the $|\varphi_\pm(k)\rangle$), the Zak phase can also be written as:

$$\gamma_0 = \int_{-\pi}^{\pi}\frac{dk}{4i}\,\text{tr}\left[\sigma_z H^{-1}_{\text{SSH}}(k)\partial_k H_{\text{SSH}}(k)\right], \tag{4}$$

and connected with the winding number ν_0 of the Bloch vector $\mathbf{d^0}$ in $H_{\text{SSH}}(k) = \mathbf{d^0}\cdot\boldsymbol{\sigma}$ in parameter space, following $\gamma_0 = \pi\nu_0$. In particular, for the

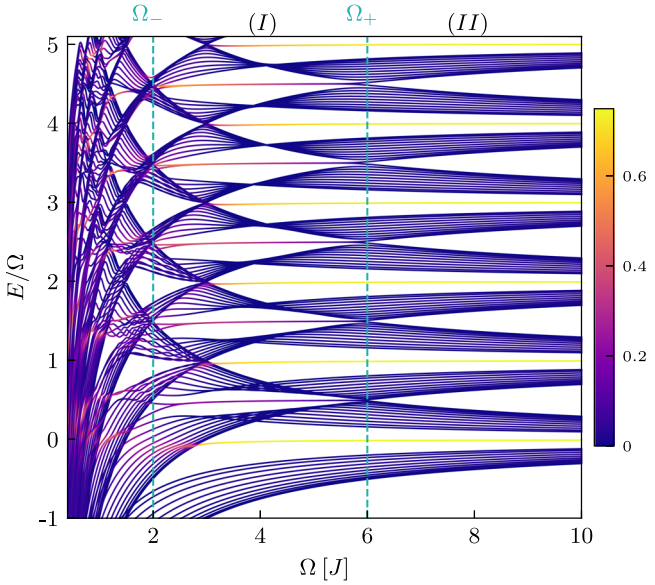

Fig. 2 | Energy spectrum of the total light-matter Hamiltonian. Light-matter energy spectrum E/Ω of a topological SSH chain ($J' = 2, J = 1$) interacting with a cavity as indicated in Hamiltonian in Eq. (1). It is plotted as a function of its frequency Ω, for a fixed light-matter interaction strength $g = 0.35$. The interaction produces resonant gaps with edge states for the range $\Omega \in [\Omega_+, \Omega_-]$, defined as $\Omega_\pm = 2|J \pm J'|$. The color code indicates localization at the edge, so that the presence of edge states is clearly visible as highly localized states, as opposed to bulk states, which showcase negligible weight on the ending sites of the chain. All plots in units of J. The chain has $N = 12$ unit cells, which corresponds to $2N$ sites. The cut-off for the photonic field is set to $n_{\max} = 50$.

unperturbed SSH chain $\nu_0 = -\Theta(J'/J - 1)$, predicting the existence of edge states for $J'>J$ (see "Methods" section).

Now we are in a position to delucidate the physics of Eq. (1) for $g \neq 0$. In Fig. 2 we plot the spectrum as a function of the cavity frequency and choose the hopping amplitudes so that the isolated chain has non-trivial topological properties ($J<J'$). The color code corresponds to the electronic localization probability, which we define as the probability of finding an electron in either one of the ending sites, $P_{1+N} = \sum_{i=1,N} |\langle i|\Psi\rangle|^2$, where $|\Psi\rangle$ corresponds to each of the eigenstates of Eq. (1). P_{1+N} should be larger for edge states, whereas for bulk states it will be negligible.

Figure 2 shows that as the cavity becomes resonant with the electronic system, additional edge states emerge within newly formed gaps between adjacent photonic bands (region *I*). It is clear that these edge states are qualitatively different from the ones appearing in the gap between the valence and the conduction band (shown in region *II*), which are linked to the ratio between hopping amplitudes ($J<J'$) and persist for high cavity frequency (region II). This is expected, since the topology of the SSH chain is approximately unaffected by the cavity at high-frequency[31], for small coupling strengths. However, important changes are produced by the non-perturbative mechanism of resonance when the cavity frequency is lowered. This scenario shows clear similarities to the anomalous Floquet phases arising in driven topological systems, with edge states appearing in the nonequivalent $0-$ and $\pi-$ gaps. However, note that in the quantum case considered here every gap in region *I* is different from each other since the interaction with the photonic field depends on the number of photons considered. This can be readily seen in the localization probability of the anomalous edge states, and how it increases as higher-energy photonic bands are considered.

We will now demonstrate that this hybrid phase with resonantly coupled photons and fermions is not topologically trivial. To proceed, first notice that if the cavity frequency is much larger than the bandwidth $2|J + J'|$, the bands in Eq. (2) are good approximations in the weak coupling regime. Therefore, it is reasonable to re-write the full Hamiltonian on this basis, and define the interaction term as the $g-$ dependent part, $V = g(d^\dagger + d)\left(b_j^\dagger a_j - a_{j+1}^\dagger b_j\right)$. With all, the Hamiltonian takes the following form:

$$\tilde{H} = \Omega d^\dagger d + \sum_{k,\nu=\pm} E_\nu(k) c_{k,\nu}^\dagger c_{k,\nu} + g\left(d + d^\dagger\right) \sum_k \sum_{\mu,\nu=\pm} V_{\mu,\nu}(k) c_{k,\mu}^\dagger c_{k,\nu}, \tag{5}$$

where $c_{k,\nu}^\dagger$ and $c_{k,\nu}$ are the creation/annihilation operators of fermionic eigenstates in the unperturbed SSH chain, and the matrix elements of the coupling between the two systems are given by $V_{\mu,\nu}(k) = \langle\varphi_\mu(k)|V|\varphi_\nu(k)\rangle$. The expressions for each component can be found in the "Methods" section. Importantly, the structure of Eq. (5) is reminiscent of that of the quantum Rabi model (QRM), where the interaction term is linear in both the fermionic and photonic operators. Note that in our case, both the longitudinal $V_{\nu,\nu}(k)$, and transversal $V_{\nu,\bar{\nu}}(k)$ coupling terms are nonzero. Importantly, as we are interested in the topology of the total system, we will neglect the diagonal contribution $V_{\nu,\nu}(k)$, as it is known that the longitudinal coupling does not alter the eigenstates of the unperturbed Hamiltonian. We will later show that this is a judicious choice that allows us to simplify the form of the Hamiltonian and obtain analytical results that capture the topological phase transitions.

Following the analogy with the QRM, and since we are mainly interested in the terms that can lead to resonances, we can also perform a Rotating Wave Approximation (RWA) on the resulting Hamiltonian, which leads to a Jaynes-Cummings (JC) Hamiltonian with a momentum dependence. Just as in the JC model, the total number of excitations is conserved, which allows us to write the Hamiltonian in a block diagonal form with basis elements: $\{|\varphi_+(k), n\rangle, |\varphi_-(k), n+1\rangle\}$:

$$\tilde{H}(n,k) = \begin{pmatrix} n\Omega + E_+(k) & -ig\Gamma(k)\sqrt{n+1} \\ ig\Gamma(k)\sqrt{n+1} & (n+1)\Omega + E_-(k) \end{pmatrix}, \tag{6}$$

where we have defined $\Gamma(k) \equiv (J + J')\sin(k)/E_+(k)$. Equation (6) can be directly diagonalized and results in the following bands:

$$\epsilon_\pm(k) = \Omega\left(n + \frac{1}{2}\right) \pm \sqrt{\left[E_+(k) - \frac{\Omega}{2}\right]^2 + g^2(n+1)\Gamma(k)^2}. \tag{7}$$

This last expression captures the $n\Omega$ separating each photonic subspace, and the Ω-dependent gap between ϵ_+ and ϵ_-. Note that the gap reduces as the resonance $\Omega = 2E_+(k)$ is approached, however, a non-zero value of the transverse light-matter coupling g prevents the gap closure by generating an anti-crossing proportional to $g^2(n+1)\Gamma(k)$.

The anti-crossing only becomes an exact crossing at the high symmetry points $k_0 = m\pi$, for $m \in \mathbb{Z}$. This is because $\Gamma(k_0) = 0$, and a crossing $2E_+(k_0) = \Omega$ will not be lifted by the interaction. Hence, we can predict the frequencies at which the gap exactly closes due to the resonance, as $\Omega_\pm = 2E_+(k_0) = 2|J \pm J'|$. Along the first Brillouin zone, this means that the gap closes at $k = 0, \pi$, respectively. Blue vertical lines in Fig. 2 indicate these values of the frequency, and one can see that they perfectly predict the appearance of additional edge states induced by the resonant coupling between the cavity and system.

To gain further intuition, we also re-write the RWA Hamiltonian for each block in the original basis, by using the explicit dependence of the eigenstates $|\phi_\pm(k)\rangle$ in terms of the original fermionic operators. This yields:

$$H(n,k) = \begin{pmatrix} \left(n + \frac{1}{2}\right)\Omega & E_+ \frac{E_+ - \frac{\Omega}{2} - ig\sqrt{n+1}\Gamma}{J + J'e^{-ik}} \\ E_+ \frac{E_+ - \frac{\Omega}{2} + ig\sqrt{n+1}\Gamma}{J + J'e^{ik}} & \left(n + \frac{1}{2}\right)\Omega \end{pmatrix}. \tag{8}$$

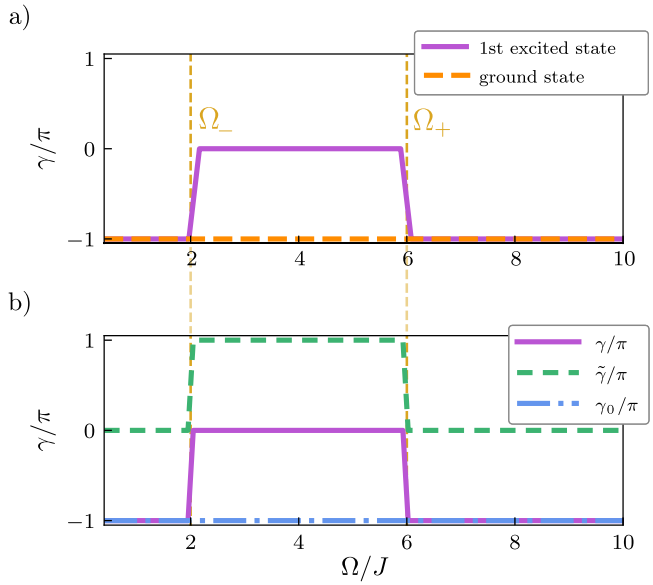

Fig. 3 | Topological invariant for the total and effective light-matter Hamiltonian. a Zak phase γ/π, as defined in Eq. (3), obtained for the total light-matter system, using the numerical eigenstates $|\Psi\rangle$ of Eq. (1). It is plotted as a function of cavity frequency Ω, for the ground (orange, dashed) and first excited state (violet, solid). **b** Zak phase γ/π, as defined in Eq. (3), obtained from the RWA effective Hamiltonian $H(n,k)$ in Eq. (8), with $n=0$ (violet curve), and contributions from the resonance $\tilde{\gamma}/\pi$ (green, dashed), and the unperturbed SSH chain ν_0 (blue, dot-dashed). The dashed, vertical lines indicate the boundaries of the region (*I*) (Fig. 2), where all gaps host edge states. All parameters are chosen as in Fig. 2: $J=1, J'=2, N=12$ J=1,J′=2,N=12 unit cells, $g=0.35$, $n_{\max}=50$.

where we have omitted the dependence on k in $E_+(k)$ and $\Gamma(k)$ for simplicity. Clearly, it retains a chiral form in each subspace, since the diagonal terms do not depend on k and just give a constant energy shift. In the high-frequency regime $\Omega \gg J, J'$, it describes copies of the SSH chain Hamiltonian, correctly predicting the topology for a largely detuned cavity. However, the off-diagonal elements now describe the hopping of polaritons, which near the resonance can strongly affect the topology due to the dominance of the term proportional to g.

Topological invariant

In order to topologically characterize the additional edge states of the system, one can extend the definition of the Zak phase for the isolated SSH chain γ_0 (or equivalently, that of the winding number ν_0) to a generalized one γ (or its generalized winding number ν). It is obtained from the light-matter eigenstates $|\Psi\rangle$ of Eq. (1) with both, photonic and fermionic parts. The numerical calculation of γ as a function of the cavity frequency is shown in Fig. 3a for the ground (orange) and first excited (violet) states. Note that it takes integer values only and that in the high-frequency regime, the topological invariant is non-vanishing for both states, in agreement with the result for the unperturbed SSH chain. However, while the ground state remains topologically non-trivial for arbitrary values of the cavity frequency, one finds that the first excited state becomes trivial when the resonance is reached. This situation reminds us of the anomalous Floquet topological phase, where with the emergence of edge states in the π-gap, the Floquet band invariant becomes trivial[13,16,17,42]. However, in our case, the system is isolated and made of fermions interacting with photons.

To understand the origin of the additional contribution to γ at resonance, we explicitly calculate the Zak phase of the hybrid eigenstates, using the eigenstates of the effective Hamiltonian in Eq. (6):

$$|\psi_\mu(k,n)\rangle\!\rangle = \alpha_\mu(k,n)|n,\varphi_+(k)\rangle + \beta_\mu(k,n)|n+1,\varphi_-(k)\rangle \tag{9}$$

with $\alpha_\pm$ and $\beta_\pm$ being the corresponding coefficients, that we can leave undetermined.

The Berry connection can be calculated to yield:

$$\begin{aligned}\mathcal{A}_{\mu,\mu} &= i\langle\psi_\mu(k,n)|\partial_k\psi_\mu(k,n)\rangle \\ &= i\alpha_\mu^*\left(\partial_k\alpha_\mu\right) + i\beta_\mu^*\left(\partial_k\beta_\mu\right) + \mathcal{A}_0,\end{aligned} \tag{10}$$

where $\mathcal{A}_\pm^0 = \langle\varphi_\pm(k)|i\partial_k|\varphi_\pm(k)\rangle$ is the Berry connection for the unperturbed SSH chain and we have used that $|\alpha_\mu|^2+|\beta_\mu|^2=1$. This shows that the connection separates in two contributions, one coming from the unperturbed SSH chain and another coming from the resonant interaction between the cavity and the chain. The latter is purely a many-body effect that entangles each band with a subspace with a different number of photons. The Zak phase is obtained by integrating the Berry connection $A_{\mu,\mu}$ over the FBZ:

$$\gamma = \tilde{\gamma} + \gamma_0, \tag{11}$$

and as it is quantized in chiral systems and $\mathcal{A}_\pm^0$ is independent of the interaction with the cavity, the new contribution from light-matter interaction $\tilde{\gamma}$, must also be quantized.

This is shown in Fig. 3b, where we plot all contributions: the violet curve corresponds to the topological invariant obtained from the effective Hamiltonian in Eq. (8) for its ground state, whereas the blue and green curves are the contributions from the unperturbed SSH $\gamma_0\pi$ and the resonant interaction $\tilde{\gamma}\pi$, respectively. It can be seen that in the resonant regime $\Omega\in[\Omega_+,\Omega_-]$, there is a one-to-one correspondence between the change in the total invariant γ/π and the contribution from the resonance $\tilde{\gamma}\pi=1$, which in combination with $\gamma_0\pi=-1$, gives to a trivial total $\gamma/\pi=0$. This might lead to the incorrect conclusion that the system is topologically trivial and therefore lacks topological edge states, which is not true, as evidenced by the energy spectrum in Fig. 2. Importantly, notice the perfect agreement between the violet curves appearing in Fig. 2a and b. First of all, note the Hamiltonian $\tilde{H}(n,k)$ in Eq. (8) does not include the ground state of the total system, just as the regular Jaynes-Cummings model does not include the ground state where neither the emitter nor the photonic field are excited. This confirms that the RWA Hamiltonian correctly describes the relevant physics for the topological changes. This further explains why the topology of the ground state for the total light-matter Hamiltonian remains unaffected by the interaction (see orange curve in Fig. 3a): the state $|\varphi_-, n=0\rangle$ is completely decoupled from the rest.

The change in the invariant can also be understood graphically. Because of the chiral form of $H(n,k)$, the winding number ν can be used for the topological characterization as well. In Fig. 4a, we plot the trajectory of the Bloch vector $\mathbf{d}(k)$ in $H(n,k)=\mathbf{d}(k)\cdot\boldsymbol{\sigma}$, as k is varied across the First Brillouin Zone. We choose different cavity frequencies, $\Omega/J=[4,\ 6,\ 7]$ (corresponding to the curves (1), (2), and (3), respectively), to visualize the topological phase transitions shown in Fig. 3. The color gradient helps visualize the direction of the curve as k changes. In Fig. 4b, we plot the trajectory for $\tilde{d}(k)$ in $\tilde{H}(n,k)=\tilde{\mathbf{d}}(k)\cdot\boldsymbol{\sigma}$ (note that $\tilde{H}(n,k)$ must be previously rotated to the $x-y$ plane to do so). Fig. 4c corresponds to the trajectory of $\mathbf{d}^0$ in $H_{\rm SSH}=\mathbf{d}^0\cdot\boldsymbol{\sigma}$, which is only dependent on the value of the hopping amplitudes (as before, they are chosen again such that the chain is in its non-trivial topological phase). At high frequency, the topology of the hybrid system, given by curve (3) in Fig. 4a, is identical to that of the unperturbed SSH chain. Their trajectories enclose the origin counterclockwise, resulting in $\nu=\nu_0=-1$. Note that, simultaneously, curve (3) in Fig. 4b has a trivial winding $\tilde{\nu}=0$. However, curve (1) in Fig. 4a ($\Omega_-<\Omega<\Omega_+$) has $\nu=0$, accounting for the additional contribution coming from $\tilde{\nu}$ with opposite sign. By canceling each other, they predict a total trivial topological phase[50].

From these findings, we can conclude that the winding number of $H(k,n)$ is not a good topological invariant to characterize the presence of topological edge states. Instead, it must be separated into two contributions,

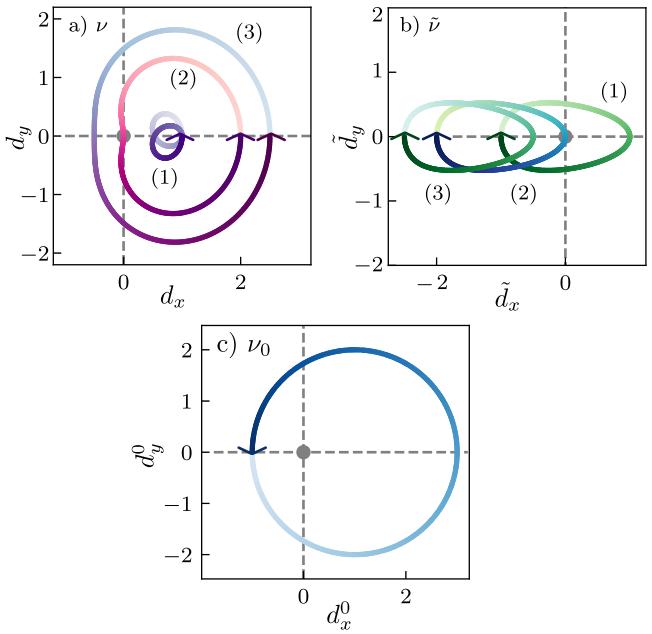

Fig. 4 | Topological invariant as winding number. Trajectory of Bloch vectors in parameter space for **a** $H(n, k)$, **b** $\tilde{H}(n, k)$, and **c** $H_{\mathrm{SSH}}(k)$, for different cavity frequencies: $\Omega/J = [4, 6, 7]$ (corresponding to curves (1), (2), and (3), respectively). We set $n = 0$ for (**a** and **b**). The color gradient helps to visualize the curve direction as k is swept across the Brillouin zone. All parameters are chosen as in Fig. 2: $J = 1, J' = 2, N = 12$J=1,J′=2,N=12 unit cells, $g = 0.35, n_{\mathrm{max}} = 50$.

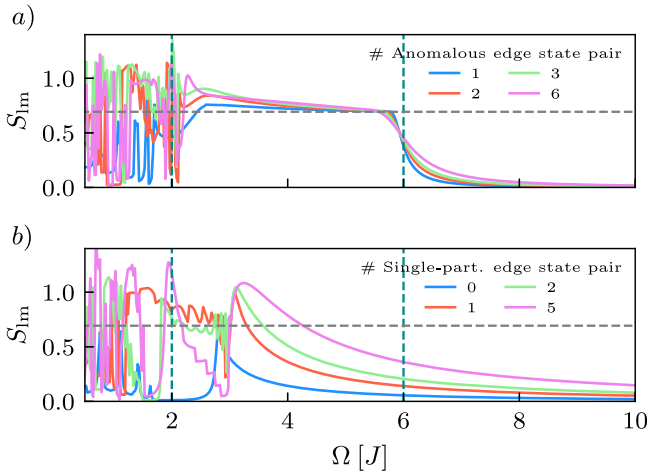

Fig. 5 | Light-matter entanglement S_{lm} for both anomalous and single-particle edge states. a S_{lm} for anomalous edge states. The numbers in the legend correspond to the position of each anomalous edge state pair in the energy spectrum, starting from the 1 pair being at the resonant gap of the lowest energy. **b** S_{lm} for the single-particle edge state. Again, the numbers correspond to the position of the single-particle edge states in the energy spectrum, which can be easily identified in the high-frequency limit. All parameters are chosen as in Fig. 2: $J = 1, J' = 2, N = 12$ unit cells, $g = 0.35, n_{\mathrm{max}} = 50$.

one corresponding to the winding number of the unperturbed SSH chain ν_0 and another to the winding number $\tilde{\nu}$, corresponding to the RWA Hamiltonian in the eigenstates basis, Eq. (6). This invariant is quantized and unambiguously predicts the appearance of edge states in the gaps created by the light-matter resonant interaction.

Light-matter entanglement

So far, we have seen that quantum anomalous topological phases emerge when the material is originally in a non-trivial topological phase and the cavity frequency is tuned to resonance with the band transitions. In that situation, photons interact with the topological system and polaritons are formed, and under the RWA approximation, this interaction can be analytically studied by the effective Hamiltonian in Eq. (6). The formation of polaritons can strongly affect the topological properties of the system, resulting in the creation of anomalous edge states in the additional gaps opened by the resonant interaction.

Now, it can be easily shown that these anomalous edge states are in fact made of maximally entangled light and matter degrees of freedom, by obtaining the entanglement entropy between both subsystems $S_{\mathrm{lm}} = -\mathrm{Tr}\{\rho_{\mathrm{l}} \log \rho_{\mathrm{l}}\}$, where $\rho_{\mathrm{l}} = \mathrm{Tr}_{\mathrm{m}}\{\rho_{\mathrm{lm}}\}$ is the reduced density matrix for the cavity and m indicates that the trace has been taken over the matter degrees of freedom. The results are shown in Fig. 5, where we plot S_{lm} as a function of the cavity frequency, considering that the system is prepared in either Fig. 5a an anomalous edge state, and Fig. 5b a single-particle edge state. The anomalous edge states show a robust entanglement structure, close to the value $S_{\mathrm{lm}} = \log 2$ (dashed, gray line in the plot), which indicates that it is a maximally entangled state. The slight deviations from this value can be explained by finite-size effects and the small contribution of other bulk states. The behavior of single-particle states is completely different, as the entanglement decays monotonically as the high-frequency regime is approached.

This result on light-matter entanglement allows us to better understand the connection between anomalous topological phases of Floquet systems and topological phases in c-QED materials. If the semi-classical limit is taken in Eq. (1), the presence of single-particle edge states can be reproduced by an effective matter Hamiltonian even after the photons are traced out, because light-matter entanglement is not relevant. This is precisely the case of high-frequency expansions that are typically used in Floquet engineering, which yield a photo-dressed Hamiltonian for the matter part only when the stroboscopic dynamics are looked at. On the contrary, the presence of maximal entanglement in the anomalous edge states means that photons cannot be safely traced out of the total system, and that, when the semi-classical limit is taken, micromotion (i.e., short-term) dynamics will have an important contribution. This means that a stroboscopic effective Hamiltonian for the matter part only will not be enough to capture the physics of the system. In fact, the appearance of anomalous Floquet phases in a driven setup is linked to the impossibility of smoothly deforming the corresponding evolution operator into that of an undriven system[51].

These results shed light on the analogy between anomalous Floquet phases and their quantum counterpart, as in both cases the presence of edge states in every gap coexist with a trivial topological invariant. It is then crucial to remind ourselves that we are considering here a c-QED setup, that is, an isolated system where the total Hamiltonian is static. So it seems reasonable to ask: how is it possible that Floquet phases describe the semi-classical limit of c-QED materials if, without quasienergies, anomalous phases should not exist? The key is that c-QED materials are many-body systems, made out of both electrons and photons, and tracing out part of the system (in our case the cavity photons) can produce an effective periodically driven Hamiltonian in the matter sector. In conclusion, the interaction with a cavity can induce an emergent discrete time-translation symmetry in the matter part, which is responsible for the appearance of fully quantum anomalous topological phases, that are made of strongly hybridized light-matter degrees of freedom.

For further insight, we also plot the average photon number $\langle n \rangle$ for the anomalous edge states, as shown in Fig. 6. The vertical, dashed lines represent the boundaries of the region $[\Omega_-, \Omega_+]$, where the anomalous edge states showcase a non-integer $\langle n \rangle$. This is expected since they are made of a superposition of different Fock states. In fact, the spatial and Fock structure of these anomalous edge states $|\Psi_{\mathrm{a.s.}}\rangle$, as given by $|\langle \Psi_{\mathrm{a.s.}}|\Psi_{\mathrm{a.s.}}\rangle|^2$, is also depicted in subplot Fig. 6b. We choose one edge state from pairs 1 and 2. The index i runs over all sites of the chain, $i \in [1, 2N]$, while the color indicates the Fock subspace n which is occupied. As shown in the left plot, the anomalous edge states in gap 1 have the spatial profile of an edge state, on both the $n = 0$ and $n = 1$ Fock subspaces. Similarly, the anomalous edge states in gap 2 are

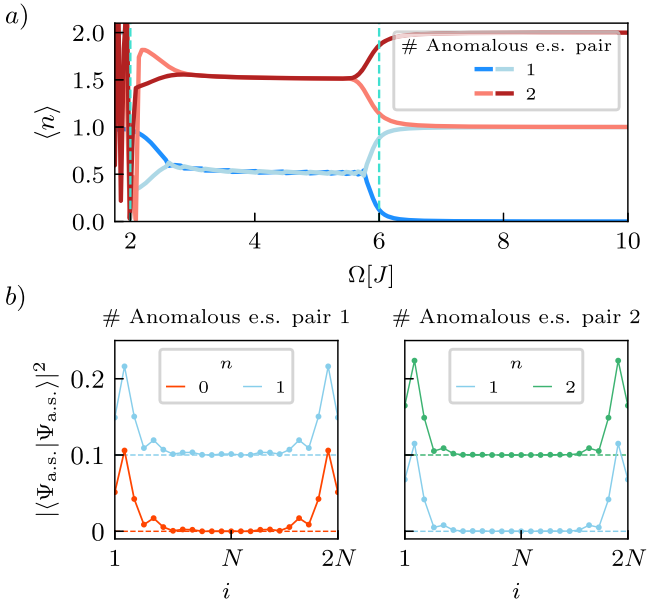

Fig. 6 | Average number of photons $\langle n\rangle$ for anomalous edge states, and spatial-light structure. a $\langle n\rangle$ is plotted for two different pairs of anomalous edge states (see legend), $\langle n\rangle$ is plotted for both edge states. The vertical, dashed lines are the boundaries of the region $[\Omega_-, \Omega_+]$. **b** Weight of the anomalous edge states on each site of the chain $i \in [1, 2N]$, for each photon subspace n (red for $n = 0$, blue for $n = 1$, and green for $n = 2$). All parameters are chosen as in Fig. 2: $J = 1, J' = 2, N = 12$ unit cells, $g = 0.35, n_{max} = 50$.

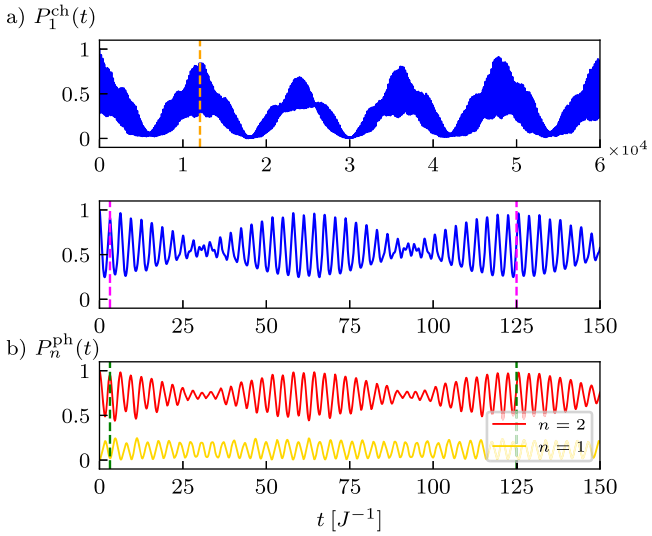

Fig. 7 | Entangled light-matter dynamics. Photon and charge dynamics, for the initial state $|1; n = 2\rangle$, considering a configuration with both anomalous and single-particle edge states. **a** Electronic occupation probability of the first site of the chain $P_1^{ch}(t)$ as a function of time, for two different time scales. The dashed, vertical lines indicate the relevant oscillation periods, as obtained from the Fourier Transform. **b** Photon dynamics $P_n^{ph}(t)$ for the subspace $n = 1$ (yellow) and $n = 2$ (red) as a function of time. In both plots, the dashed, vertical lines indicate the relevant oscillation periods. Parameters: $\Omega = 4, J' = 2, J = 1, g = 0.35, N = 8, n_{max} = 50$.

mainly defined on $n = 1$ and $n = 2$. As the high-frequency limit is approached, the anomalous edge states merge with the bulk states belonging to different photonic subspaces. Since the cavity frequency is larger than the electronic bandwidth, this means that $\langle n\rangle$ will take an integer value, approximately, as can be seen on the right-hand side of Fig. 6a.

Entangled light-matter dynamics

Charge and photon dynamics can in fact help us visualize the previous results on light-matter entanglement. A well-known result for charge dynamics in the isolated SSH chain with topological edge states is the appearance of periodic Rabi oscillations between the ending sites for a particle that is initially occupying the edge[12,52]. The frequency of the oscillation is given by the energy splitting between the edge states due to finite-size effects, while the leakage to the bulk is suppressed. Similarly, for a topological chain interacting with a highly-detuned cavity, charge, and photon dynamics are essentially decoupled: the behavior of the charge would be governed by the presence or absence of edge states, just as in the isolated chain, while for photons, no time-dependence is expected to appear[31].

This scenario, however, becomes increasingly complex when we consider the coupling to a resonant photonic field, with the presence of both single-particle and anomalous edge states. In this case, charge and photon dynamics are dominated by the fact that the edge states arising from light-matter resonances showcase a superposition of different photon numbers (see Fig. 6). Anomalous edge states have the spatial profile of conventional edge states, with the additional feature of having a non-zero weight on different photonic subspaces. This gives rise to photon dynamics and can be equated to the characteristic time-dependence of anomalous edge states in Floquet systems[44], leading to the formation of unique interference patterns in the entangled light-matter dynamics that are exclusive to the anomalous phase arising in the hybrid light-matter system.

Let us investigate charge-photon dynamics for a configuration with coexisting single-particle and anomalous edge states, by setting $\Omega = 4$ (middle part of the region *I*, Fig. 2). Let the initial state be $|1; n = 2\rangle$, where 1 refers to a charged particle occupying the first site of the chain and n refers to the number of photons. Generally speaking, three pairs of edge states will contribute the most to the charge dynamics: the pair of single-particle edge states with predominant weight on the Fock subspace $n = 2$, and the two pairs of anomalous edge states appearing in the adjacent resonant gaps, located at a distance of $\pm\Omega/2$.

The resulting dynamics for this configuration are shown in Fig. 7. For the matter part, we plot the occupation probability of the first site of the chain, $P_1^{ch}(t) = |\langle 1|U(t)|1; n = 2\rangle|^2$, as a function of time, where $U(t) = \exp(-iHt)$ corresponds to the time evolution operator. The upper plot of Fig. 7a depicts the long-term behavior of $P_1^{ch}(t)$, which showcases clear oscillations, as expected for a topological system displaying edge states. The dashed, vertical line (orange) indicates the oscillation period, which is obtained through Fourier Transform (FT) analysis (see Supplementary Fig. 1 for additional details on the FT in Supplementary Note 1). The comparison with the energy scales of the Hamiltonian confirms that this oscillation is in fact related to the energy splitting of the single-particle edge states with $\langle n\rangle \approx 2$. However, a closer inspection reveals that, for short times, $P_1^{ch}(t)$ displays a beating (lower plot of Fig. 7a), i.e., a modulated-amplitude oscillation, which is an unavoidable signature of interference between different eigenstates. Such patterns appear due to the presence of two slightly different frequencies f_1 and f_2, whose interference results in a faster oscillation with frequency $(f_1 + f_2)/2$, and amplitude modulation of frequency $|f_1 - f_2|/2$. The corresponding period of both oscillations is indicated with dashed, vertical lines (magenta), based on the results of the FT. This behavior is a result of the characteristic photon occupation of the anomalous edge states, which allows for some overlap between them and the single-particle ones. Then, the small energy differences between the single-particle and the anomalous edge states appearing in the upper and lower resonant gap give rise to two close-by frequencies that create this interference effect. Note that, in the absence of anomalous edge states, the single-particle ones are typically isolated from other eigenstates of the system,[30,31], which is the reason why the leakage to the bulk is negligible for reasonable system sizes. In subplot of Fig. 7b, we show the photon dynamics, i.e., the photon occupation of the Fock subspace n, $P_n^{ph}(t) = |\langle n|U(t)|1; n = 2\rangle|^2$. We plot this quantity for $n = 2$ (red curve), which shows the same behavior as $P_1^{ch}(t)$, as expected. Photons inherit the beating pattern as well since the oscillation between single-particle and anomalous edge states also involves

the exchange of photons. The time-dependence of $P^{\mathrm{ph}}_{n=2}(t)$ leads to the population of other Fock subspaces, as that with $n = 1$ (yellow curve).

Conclusions

In summary, our results provide a bridge between isolated, hybrid light-matter systems and periodically driven ones with classical AC fields. We have shown that anomalous Floquet topological phases can emerge in the semi-classical limit of c-QED materials and have described their quantum origin. Far from the semi-classical limit they also display edge states and trivial bands, but their physical properties are very different due to the presence of back-action and light-matter correlations. This confirms that an effective, discrete time-translation symmetry emerges in the matter sector due to the coupling to cavity photons, as otherwise anomalous topological phases could not be present.

The required ingredient to create this anomalous hybrid phase in c-QED materials is a cavity that is resonant with a topological system that already displays edge states. However, the interaction term also needs to have the right symmetry, to produce an exact crossing between different Fock subspaces.

To confirm the topological origin of this hybrid light-matter phase we have identified two topological invariants, ν_0 and $\tilde{\nu}$, which predict the presence of edge states in the single-particle and resonant gaps, respectively. One is the standard winding number of non-interacting one-dimensional chiral systems, while the other is a winding number that captures the resonant light-matter interaction. We have shown that although their sum vanishes, it is their independent value that matters and defines a light-matter invariant for the system, which establishes the correct bulk-to-boundary correspondence. Importantly, our result shows a link between the unequivalent 0 and π gaps of Floquet systems, and the single-particle and interaction-induced gaps, respectively.

Our findings could be experimentally verified on different platforms, for example, ion traps, where it should be possible to engineer the required interaction by combining longitudinal and transverse phononic degrees of freedom[53]. Importantly, phonons would need to have the right range of frequencies to produce a resonant interaction with the chain. Another possibility would be the use of superconducting circuits[54], where the coupling to the cavity can be simulated by additional waveguides. Dimerization can be obtained by locally changing the capacitance in the LRC circuits[55].

Lastly, we can envision future research lines based on our results, such as the extension to other non-trivial topological systems, as the Creutz ladder or other quasi-one-dimensional ladder models[56].

Methods

Derivation of the effective Hamiltonian

The effective Hamiltonian can be directly derived from the original Hamiltonian in Eq. (1). The first step is to find the eigenvectors $|\varphi_{\pm}(k)\rangle$ of $\mathcal{H}_{\mathrm{SSH}}(k)$, obtained from the unperturbed SSH chain Hamiltonian with PBC, $H_{\mathrm{SSH}} = \sum_k \Psi_k^{\dagger}\mathcal{H}_{\mathrm{SSH}}(k)\Psi_k$, with:

$$\mathcal{H}_{\mathrm{SSH}}(k) = \begin{pmatrix} 0 & J + J'e^{ik} \\ J + J'e^{-ik} & 0 \end{pmatrix} \tag{12}$$

and $\Psi_k = (a_k, b_k)$. The corresponding eigenvalues are given in Eq. (2). Then, rewriting the full Hamiltonian in this basis for the fermionic part, we arrive at Eq. (5). In particular, the matrix elements of the coupling between the two systems are given by the following expressions:

$$V_{+,+}(k) = \frac{(1-\cos(k))(J-J')}{\sqrt{J^2 + J'^2 + 2JJ'\cos(k)}} \tag{13}$$

$$V_{+,-}(k) = \frac{-i\sin(k)(J+J')}{\sqrt{J^2 + J'^2 + 2JJ'\cos(k)}} = -i\Gamma(k) \tag{14}$$

$$V_{-,+}(k) = \frac{i\sin(k)(J+J')}{\sqrt{J^2 + J'^2 + 2JJ'\cos(k)}} = i\Gamma(k) \tag{15}$$

$$V_{-,-}(k) = -\frac{(1-\cos(k))(J-J')}{\sqrt{J^2 + J'^2 + 2JJ'\cos(k)}} \tag{16}$$

Calculation of the topological invariant

Starting from the simplest case of the unperturbed SSH chain, where chiral symmetry is given by a σ_z operator, we can obtain the Berry connection from the eigenstates of H_{SSH}, $|\varphi_{\mu}\rangle$:

$$\mathcal{A}_0 = \langle\varphi_{\mu}|i\partial_k|\varphi_{\mu}\rangle = -\frac{J'[J\cos(k) + J']}{2\left[J^2 + J'^2 + 2JJ'\cos(k)\right]} \tag{17}$$

Interestingly, the expression is identical for the two eigenstates. This is the reason why the calculation of the Zak phase, by integrating over the whole FBZ, results in the same values for both (we define $z \equiv e^{ik}$):

$$\gamma_0 = -\oint \frac{dz}{4i}\frac{z^2 + 2\frac{J'}{J}z + 1}{z(z-z_+)(z-z_-)} = -\pi\Theta(1 - J/J') \tag{18}$$

being $\Theta(x)$ the Heaviside function and the integral in the complex plane over the unit circle. This demonstrates that for the SSH chain, the Zak phase is quantized in the topological phase, $J<J'$.

Because the system has chiral symmetry, it is also possible to directly calculate the winding number from the Hamiltonian:

$$\nu_0 = \int_{-\pi}^{\pi} \mathrm{tr}\left\{\sigma_z H^{-1}_{\mathrm{SSH}}\partial_k H_{\mathrm{SSH}}\right\}\frac{dk}{4\pi i} = -\Theta(1 - J/J'), \tag{19}$$

which coincides with the expression from the Zak phase, divided by π. This particular feature allows us to relate the quantized Zak phase with the value of the winding number via the relation $\gamma_0 = \pi\nu_0$.

This relation between the Zak phase and the winding number can be extended to the many-body Zak phase, if the many-body system is also chiral, as in our present case. To calculate the many-body Zak phase we consider a momentum space discretization and calculate the infinitesimal rotation of many-body eigenstates, $|\Psi_{\mu}(k)\rangle$, as they are parallel transported along the FBZ. Summing over all contributions we arrive at:

$$\gamma_{\mu} = -\sum_{k=-\pi}^{\pi-\delta k} \mathrm{Im}\left\{\log\left[\langle\Psi_{\mu}(k)|\Psi_{\mu}(k+\delta k)\rangle\right]\right\}, \tag{20}$$

and define $\nu_{\mu} = \gamma_{\mu}/\pi$. Notice that now the index μ of the many-body eigenstates runs over all many-body eigenstates.

To complete the description of the topological phases, and in particular of the phase with many-body edge states and vanishing winding number, we focus on the analytically solvable model of Eq. (8). The Hamiltonian is the basis of eigenstates of H_{SSH} and because it is chiral, its winding number for each subspace can be calculated with an identical formula. Notice however that in order to use the same chiral operator, σ_z, one must perform a rotation of the Hamiltonian. Similarly, from its eigenstates, one can calculate the Zak phase analytically, or numerically. All this gives the same result for $\tilde{\nu}$.

Code availability

The code to reproduce the figures and numerical calculations of this work can be found in (B. Pérez-González (2024), https://doi.org/10.5281/zenodo.13353498).

Received: 21 April 2024; Accepted: 5 December 2024;
Published online: 21 December 2024

References

1. Laughlin, R. B. Quantized hall conductivity in two dimensions. *Phys. Rev. B* **23**, 5632–5633 (1981).
2. Thouless, D. J., Kohmoto, M., Nightingale, M. P. & den Nijs, M. Quantized hall conductance in a two-dimensional periodic potential. *Phys. Rev. Lett.* **49**, 405–408 (1982).
3. Klitzing, K. V., Dorda, G. & Pepper, M. New method for high-accuracy determination of the fine-structure constant based on quantized hall resistance. *Phys. Rev. Lett.* **45**, 494–497 (1980).
4. Ma, S. & Anlage, S. M. Microwave applications of photonic topological insulators. *Appl. Phys. Lett.* **116**, 250502 (2020).
5. Gilbert, M. J. Topological electronics. *Commun. Phys.* **4**, 70 (2021).
6. Lindner, N. H., Refael, G. & Galitski, V. Floquet topological insulator in semiconductor quantum wells. *Nat. Phys.* **7**, 490–495 (2011).
7. Kitagawa, T., Oka, T., Brataas, A., Fu, L. & Demler, E. Transport properties of nonequilibrium systems under the application of light: Photoinduced quantum hall insulators without landau levels. *Phys. Rev. B* **84**, 235108 (2011).
8. Gómez-León, A. & Platero, G. Floquet-bloch theory and topology in periodically driven lattices. *Phys. Rev. Lett.* **110**, 200403 (2013).
9. Delplace, P., Gómez-León, A. & Platero, G. Merging of Dirac points and Floquet topological transitions in ac-driven graphene. *Phys. Rev. B* **88**, 245422 (2013).
10. Grushin, A. G., Gómez-León, A. & Neupert, T. Floquet fractional Chern insulators. *Phys. Rev. Lett.* **112**, 156801 (2014).
11. Perez-Piskunow, P. M., Usaj, G., Balseiro, C. A. & Torres, L. E. F. F. Floquet chiral edge states in graphene. *Phys. Rev. B* **89**, 121401 (2014).
12. Pérez-González, B., Bello, M., Platero, G. & Gómez-León, A. Simulation of 1d topological phases in driven quantum dot arrays. *Phys. Rev. Lett.* **123**, 126401 (2019).
13. Rudner, M. S., Lindner, N. H., Berg, E. & Levin, M. Anomalous edge states and the bulk-edge correspondence for periodically driven two-dimensional systems. *Phys. Rev. X* **3**, 031005 (2013).
14. Gómez-León, A., Delplace, P. & Platero, G. Engineering anomalous quantum hall plateaus and antichiral states with ac fields. *Phys. Rev. B* **89**, 205408 (2014).
15. Quelle, A., Weitenberg, C., Sengstock, K. & Morais Smith, C. Driving protocol for a Floquet topological phase without static counterpart. *New J. Phys.* **19**, 113010 (2017).
16. Rudner, M. S. & Lindner, N. H. Band structure engineering and non-equilibrium dynamics in Floquet topological insulators. *Nat. Rev. Phys.* **2**, 229–244 (2020).
17. Gómez-León, Á. Anomalous floquet phases. A resonance phenomena. *Quantum* **8**, 1522 (2024).
18. Forn-Díaz, P. et al. Observation of the Bloch-Siegert shift in a qubit-oscillator system in the ultrastrong coupling regime. *Phys. Rev. Lett.* **105**, 237001 (2010).
19. Niemczyk, T. et al. Circuit quantum electrodynamics in the ultrastrong-coupling regime. *Nat. Phys.* **6**, 772–776 (2010).
20. Yoshihara, F. et al. Superconducting qubit–oscillator circuit beyond the ultrastrong-coupling regime. *Nat. Phys.* **13**, 44–47 (2017).
21. Frisk Kockum, A., Miranowicz, A., De Liberato, S., Savasta, S. & Nori, F. Ultrastrong coupling between light and matter. *Nat. Rev. Phys.* **1**, 19–40 (Springer US, 2019).
22. Romero, G., Ballester, D., Wang, Y. M., Scarani, V. & Solano, E. Ultrafast quantum gates in circuit QED. *Phys. Rev. Lett.* **108**, 120501 (2012).
23. Schlawin, F., Kennes, D. M. & Sentef, M. A. Cavity quantum materials. *Appl. Phys. Rev.* **9**, 011312 (2022).
24. Sentef, M. A., Li, J., Künzel, F. & Eckstein, M. Quantum to classical crossover of Floquet engineering in correlated quantum systems. *Phys. Rev. Res.* **2**, 033033 (2020).
25. Bomantara, R. W. & Gong, J. Generating controllable type-II weyl points via periodic driving. *Phys. Rev. B* **94**, 235447 (2016).
26. Li, J. & Eckstein, M. Manipulating intertwined orders in solids with quantum light. *Phys. Rev. Lett.* **125**, 217402 (2020).
27. Li, J., Schamriß, L. & Eckstein, M. Effective theory of lattice electrons strongly coupled to quantum electromagnetic fields. *Phys. Rev. B* **105**, 165121 (2022).
28. Dmytruk, O. & Schiro, M. Controlling topological phases of matter with quantum light. *Commun. Phys.* **5**, 271 (2022).
29. Eckhardt, C. J. et al. Quantum Floquet engineering with an exactly solvable tight-binding chain in a cavity. *Commun. Phys.* **5**, 122 (2022).
30. Pérez-González, B., Gómez-León, A. & Platero, G. Topology detection in cavity QED. *Phys. Chem. Chem. Phys.* **24**, 15860–15870 (2022).
31. Pérez-González, B., Platero, G. & Gómez-León, Á. Light-matter correlations in quantum Floquet engineering. *arXiv preprint arXiv:2302.12290* (2023).
32. Shirley, J. H. Solution of the Schrödinger equation with a Hamiltonian periodic in time. *Phys. Rev.* **138**, B979–B987 (1965).
33. Roy, R. & Harper, F. Periodic table for Floquet topological insulators. *Phys. Rev. B* **96**, 155118 (2017).
34. Su, W. P., Schrieffer, J. R. & Heeger, A. J. Solitons in polyacetylene. *Phys. Rev. Lett.* **42**, 1698–1701 (1979).
35. Heeger, A. J., Kivelson, S., Schrieffer, J. R. & Su, W. P. Solitons in conducting polymers. *Rev. Mod. Phys.* **60**, 781–850 (1988).
36. Jackiw, R. & Rebbi, C. Solitons with fermion number 1/2. *Phys. Rev. D.* **13**, 3398–3409 (1976).
37. Pérez-González, B., Bello, M., Gómez-León, A. & Platero, G. Interplay between long-range hopping and disorder in topological systems. *Phys. Rev. B* **99**, 035146 (2019).
38. Dal Lago, V., Atala, M. & Foa Torres, L. E. F. Floquet topological transitions in a driven one-dimensional topological insulator. *Phys. Rev. A* **92**, 023624 (2015).
39. Olin, S. & Lee, W.-C. Topological phase transition in the commensurate multifrequency floquet Su-Schrieffer-Heeger model. *Phys. Rev. B* **107**, 094310 (2023).
40. Asbóth, J. K., Tarasinski, B. & Delplace, P. Chiral symmetry and bulk-boundary correspondence in periodically driven one-dimensional systems. *Phys. Rev. B* **90**, 125143 (2014).
41. Eckardt, A. & Anisimovas, E. High-frequency approximation for periodically driven quantum systems from a Floquet-space perspective. *N. J. Phys.* **17**, 093039 (2015).
42. Balabanov, O. & Johannesson, H. Robustness of symmetry-protected topological states against time-periodic perturbations. *Phys. Rev. B* **96**, 035149 (2017).
43. Cardano, F. et al. Detection of zak phases and topological invariants in a chiral quantum walk of twisted photons. *Nat. Commun.* **8**, 15516 (2017).
44. Cheng, Q. et al. Observation of anomalous π modes in photonic Floquet engineering. *Phys. Rev. Lett.* **122**, 173901 (2019).
45. Kitagawa, T., Berg, E., Rudner, M. & Demler, E. Topological characterization of periodically driven quantum systems. *Phys. Rev. B* **82**, 235114 (2010).
46. Wu, S. et al. Anomalous π modes by Floquet engineering in optical lattices with long-range coupling. *Opt. Express* **30**, 44983–44991 (2022).
47. Berry, M. V. Quantal phase factors accompanying adiabatic changes. *Proc. R. Soc. Lond. A. Math. Phys. Sci.* **392**, 45–57 (1984).
48. Zak, J. Berry's phase for energy bands in solids. *Phys. Rev. Lett.* **62**, 2747–2750 (1989).
49. Atala, M. et al. Direct measurement of the Zak phase in topological Bloch bands. *Nat. Phys.* **9**, 795–800 (2013).
50. Downing, C. A., Sturges, T. J., Weick, G., Stobińska, M. & Martín-Moreno, L. Topological phases of polaritons in a cavity waveguide. *Phys. Rev. Lett.* **123**, 217401 (2019).

51. Nathan, F. & Rudner, M. S. Topological singularities and the general classification of Floquet-Bloch systems. *New J. Phys.* **17**, 125014 (2015).
52. Bello, M., Creffield, C. E. & Platero, G. Long-range doublon transfer in a dimer chain induced by topology and ac fields. *Sci. Rep.* **6**, 22562 (2016).
53. Nevado, P., Fernández-Lorenzo, S. & Porras, D. Topological edge states in periodically driven trapped-ion chains. *Phys. Rev. Lett.* **119**, 210401 (2017).
54. Kim, E. et al. Quantum electrodynamics in a topological waveguide. *Phys. Rev. X* **11**, 011015 (2021).
55. Yu, X.-L. et al. Topological phase transitions, Majorana modes, and quantum simulation of the Su–Schrieffer–Heeger model with nearest-neighbor interactions. *Phys. Rev. B* **101**, 045422 (2020).
56. Zurita, J., Creffield, C. & Platero, G. Tunable zero modes and quantum interferences in flat-band topological insulators. *Quantum* **5**, 591 (2021).

Acknowledgements

We acknowledge support from the European Union's Horizon2020 research and innovation program under Grant Agreement No.899354(SuperQuLAN), the Proyecto Sinergico CAM 2020 Y2020/TCS-6545 (NanoQuCoCM), and from CSIC Interdisciplinary Thematic Platform (PTI+) on Quantum Technologies (PTI-QTEP+). GP and BPG are supported by Spain's MINECO through Grant No. PID2020-117787GB-I00 and by the CSIC Research Platform PTI-001. G P and BPG also acknowledge the agreement between Carlos III University and the CSIC through the UA.

Author contributions

B.P.G. and A.G.L. did the analytical and numerical analysis. B.P.G., A.G.L., and G.P. discussed and analyzed the results, and contributed to the writing of the manuscript.

Competing interests

The authors declare no competing interests.

Additional information

Supplementary information The online version contains supplementary material available at https://doi.org/10.1038/s42005-024-01908-y.

Correspondence and requests for materials should be addressed to Beatriz Pérez-González, Gloria Platero or Álvaro Gómez-León.

Peer review information *Communications Physics* thanks Yiming Pan and the other, anonymous, reviewer(s) for their contribution to the peer review of this work. A peer review file is available.